J. Biophotonics **9**, No. 4, 388–395 (2016) / **DOI** 10.1002/jbio.201500131

Journal of BIOPHOTONICS

FULL ARTICLE

Wavelength-Modulated Differential Photoacoustic Spectroscopy (WM-DPAS) for noninvasive early cancer detection and tissue hypoxia monitoring

Sung soo (Sean) Choi[1], *Andreas Mandelis*[*, 1, 2], *Xinxin Guo*[1], *Bahman Lashkari*[1], *Stephan Kellnberger*[2], *and Vasilis Ntziachristos*[2]

[1] Center for Advanced Diffusion-Wave Technologies, Department of Mechanical and Industrial Engineering, University of Toronto, 5 King's College Road, Toronto ON M5S 3G8, Canada
[2] Institute for Biological and Medical Imaging, Technische Universität München and Helmholtz Zentrum München, Ingolstädter Landstraße 1, 85764 Neuherberg, Germany

Received 24 March 2015, revised 2 May 2015, accepted 4 May 2015
Published online 22 May 2015

Key words: differential photoacoustic, biosensor, noninvasive, premalignant, hypoxia

This study introduces a novel noninvasive differential photoacoustic method, Wavelength Modulated Differential Photoacoustic Spectroscopy (WM-DPAS), for noninvasive early cancer detection and continuous hypoxia monitoring through ultrasensitive measurements of hemoglobin oxygenation levels (StO_2). Unlike conventional photoacoustic spectroscopy, WM-DPAS measures simultaneously two signals induced from square-wave modulated laser beams at two different wavelengths where the absorption difference between maximum deoxy- and oxyhemoglobin is 680 nm, and minimum (zero) 808 nm (the isosbestic point). The two-wavelength measurement efficiently suppresses background, greatly enhances the signal to noise ratio and thus enables WM-DPAS to detect very small changes in total hemoglobin concentration (C_{Hb}) and oxygenation levels, thereby identifying pre-malignant tumors before they are anatomically apparent. The non-invasive nature also makes WM-DPAS the best candidate for ICU bedside hypoxia monitoring in stroke patients. Sensitivity tunability is another special feature of the technology: WM-DPAS can be tuned for different applications such as quick cancer screening and accurate StO_2 quantification by selecting a pair of parameters, signal amplitude ratio and phase shift. The WM-DPAS theory has been validated with sheep blood phantom measurements.

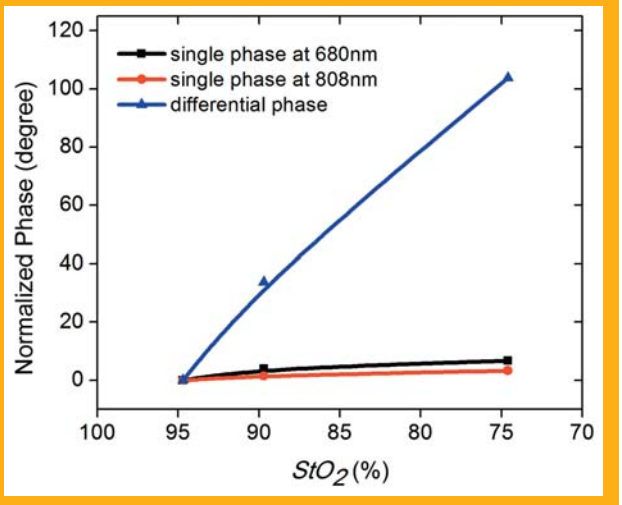

Sensitivity comparison between conventional single-ended signal and differential signal.

* Corresponding author: e-mail: mandelis@mie.utoronto.ca, Phone: +1 416 978 5106, Fax: +1 416 978 7753

1. Introduction

Tissue hypoxia, a state of depressed oxygen tension, is of great clinical importance because it is associated with tumor propagation, malignant progression, and resistance to therapy [1, 2]. It has become a hallmark in cancer diagnostics and a central issue in cancer treatment [2]. The assessment of tissue oxygenation level is also essential to stroke patient management. Real-time monitoring of cerebral StO_2 after the initial few hours and over the next few days improves stroke patient recovery outcomes [3]. The present "gold standard" for the detection and characterization of tumor hypoxia is intratumor polarographic electrodes [1, 2]. However, their clinical use is severely hampered by their invasive nature, high variability and low sample specificity [4]. Several alternative modalities exist for assessing tumor hypoxia by utilizing various mechanisms, for example Phosphorescence Quenching [5], Electron Paramagnetic Resonance (EPR) [6], ^{19}F-Magnetic Resonance Spectroscopy (MRS) [7] and Overhauser-enhanced MRI (OMRI) (8), yet no single modality is approved for assessing tumor hypoxia in routine clinical practice [1]. New methods, especially noninvasive ones, for accurately assessing tissue hypoxia are in acute need for both hypoxia diagnosis and therapy development. The potential noninvasive methods include Near-infrared Spectroscopy/Tomography (NIR) and Photoacoustic Tomography (PAT). NIR relies on the different absorption spectra of deoxy-hemoglobin (Hb) and oxy-hemoglobin (HbO_2) to quantify a ratio of Hb/HbO_2 [9]. One variation of this method, Diffuse Optical Tomography (DOT), was used to reconstruct the 3D oxygen distribution in breast cancer patients [10]. But the method is limited by shallow tissue penetration and lack of spatial resolution. PAT is an ultrasound based imaging modality that detects sound waves generated from absorbed light. The combination of high structural resolution and optical contrast with excellent depth penetration makes this imaging modality a promising technique for hypoxia assessment [11, 12]. However, due to the optical heterogeneities in tissue, quantification of local fluence F in units of J/m^2 is challenging. Even though multiple methods have been proposed to address the problem [13–16], the required sophisticated modeling makes real-time imaging difficult. Here we propose a differential photoacoustic method Wavelength Modulated Differential Photoacoustic Spectroscopy (WM-DPAS) for accurate tissue hypoxia quantification. Unlike conventional PAT, WM-DPAS measures at two laser wavelengths (680 nm and 808 nm) simultaneously, thus canceling the local fluence variations, eliminating background noise and yielding high sensitivity and specificity.

2. Theory

2.1 PA signal evolution equations

A recent study published elsewhere [17] reported the effects of various waveform modulations on the SNR of the PA signal. It was shown that square-wave modulation produced stronger PA signal than other waveforms (sine-wave and pulse train) due to the differences in the frequency spectrum of the excitation signal involved in PA generation. Therefore, the development of the WM-DPAS system relied on two out-of-phase single frequency square-wave modulated optical sources.

Generation of the PA signal from tissue chromophores depends on a number of factors at both the optical and absorber ends. Assuming that a single period of a square-wave modulated optical waveform from laser A is absorbed by a semi-infinite subsurface absorber with absorption coefficient, μ_a, at depth L_1 below the surface of the scattering medium (effective attenuation coefficient, μ_{eff}), the generated single-ended PA signal $P_{sA}(t)$ can be expressed as,

$$P_{sA}(t) = C_A \times \left[H\left(\frac{\tau_0}{2} - t\right) - e^{-\mu_{aA} v_a t} + e^{-\mu_{aA} v_a \left(t - \frac{\tau_0}{2}\right)} H\left(t - \frac{\tau_0}{2}\right)\right]; \quad 0 \le t \le \tau_0 \tag{1}$$

$$C_A = \frac{I_{0A} \beta_a v_a \, e^{-\mu_{\text{eff}A} L_1}}{C_p}$$

$$H(y) = \begin{cases} 1; y > 0 \\ 0; y < 0 \end{cases} \tag{1.1}$$

where C_A and $H(y)$ are a constant factor for laser A wavelength and the Heaviside step function respectively as described in Eq. (1.1). I_{0A} is the optical intensity of laser A in W/m^2, β_a is the thermoelastic expansion coefficient in K^{-1}, v_a is the speed of sound in the absorber in m/s, C_p is the specific heat of the target in $J/kg \cdot K$, and τ_0 is the modulation period. In reality, multiple periods of optical waveforms are used, so the accumulated signal contributions from previous periods to the present period must be considered. As the single-ended PA signal from each of the previous periods can be represented as:

$$P_{sA-0}(t) = C_A \times \left[H\left(\frac{\tau_0}{2} - t\right) - e^{-\mu_{aA} v_a t} + e^{-\mu_{aA} v_a \left(t - \frac{\tau_0}{2}\right)} H\left(t - \frac{\tau_0}{2}\right)\right]; \quad 0 \le t \le \tau_0$$

$$P_{sA-1}(t) = C_A\left[e^{-\mu_{aA}v_a\left(t+\tau_0-\frac{\tau_0}{2}\right)} - e^{-\mu_{aA}v_a(t+\tau_0)}\right];$$
$$0 \le t \le \tau_0$$
$$P_{sA-2}(t) = C_A\left[e^{-\mu_{aA}v_a\left(t+2\tau_0-\frac{\tau_0}{2}\right)} - e^{-\mu_{aA}v_a(t+2\tau_0)}\right];$$
$$0 \le t \le \tau_0$$
$$\vdots \text{ N}^{\text{th}} \text{ period}$$
$$P_{sA-N}(t) = C_A\left[e^{-\mu_{aA}v_a\left(t+\frac{2N-1}{2}\tau_0\right)} - e^{-\mu_{aA}v_a(t+N\tau_0)}\right];$$
$$0 \le t \le \tau_0$$

the total signal from laser A, $P_A(t)$, can be expressed as:

$$P_A(t) = C_A\left\{H\left(\frac{\tau_0}{2}-t\right).\right.$$
$$+\sum_{N=0}^{\infty}\left[e^{-\mu_{aA}v_a\left(t+\frac{2N-1}{2}\tau_0\right)}H\left(t+\frac{2N-1}{2}\tau_0\right)\right.$$
$$\left.\left.-e^{-\mu_{aA}v_a(t+N\tau_0)}\right]\right\};$$
$$0 \le t \le \tau_0 \quad (2)$$

The PA signal which is generated when the single period of square-wave modulated waveform from laser B is absorbed by the same sample can be similarly represented as Eq. (1), but a 180° phase shift with respect to the modulation waveform of laser A should be taken into account in a differential system; that is:

$$P_{sB}(t) = C_B\left\{e^{-\mu_{aB}v_at} - e^{-\mu_{aB}v_a\left(t+\frac{\tau_0}{2}\right)}\right.$$
$$\left.+\left[1-e^{-\mu_{aB}v_a\left(t-\frac{\tau_0}{2}\right)}\right]H\left(t-\frac{\tau_0}{2}\right)\right\};$$
$$0 \le t \le \tau_0 \quad (3)$$

$$C_B = \frac{I_{0B}\beta_a v_a\, e^{-\mu_{effB}L_1}}{C_{pa}} \quad (3.1)$$

where C_B is the respective constant factor for laser B wavelength and I_{0B} is the optical intensity of laser B in W/m^2. When the contributions of the previous periods are taken into account, the total signal from laser B, $P_B(t)$, is:

$$P_B(t) = C_B\left\{\sum_{N=0}^{\infty} e^{-\mu_{aB}v_a(t+N\tau_0)} - e^{-\mu_{aB}v_a\left(t+\frac{2N+1}{2}\tau_0\right)}\right.$$
$$\left.+\left[1-e^{-\mu_{aB}v_a\left(t-\frac{\tau_0}{2}\right)}\right]H\left(t-\frac{\tau_0}{2}\right)\right\};$$
$$0 \le t \le \tau_0 \quad (4)$$

To adjust the phase shift of the PA signal from laser B to an angle other than 180°, a time delay $\pm\Delta t$ can be added to Eq. (4) as:

$$P_B(t) = C_B\left\{\sum_{N=0}^{\infty}\left[e^{-\mu_{aB}v_a(t+\Delta t+N\tau_0)} - e^{-\mu_{aB}v_a\left(t+\Delta t+\frac{2N+1}{2}\tau_0\right)}\right]\right.$$
$$\left.+\left[1-e^{-\mu_{aB}v_a\left(t+\Delta t-\frac{\tau_0}{2}\right)}\right]H\left(t+\Delta t-\frac{\tau_0}{2}\right)\right\};$$
$$0 \le t \le \tau_0 \quad (5)$$

When these two PA signals from laser A and laser B are superimposed, the differential PA signal equation can be simply derived by adding Eqs. (2) and (4) or (5) as:

$$P_{AB}(t) = P_A(t) + P_B(t). \quad (6)$$

2.2 Biomedical applications

The WM-DPAS theory assumes two lasers of different wavelengths (λ_A = 680 nm and λ_B = 808 nm) where two waveforms are square-wave modulated at around 180° phase difference. Two specific wavelengths have been chosen based on the hemoglobin (Hb) absorption spectrum (Figure 1) so that, at 680 nm, the molar extinction coefficients of oxy- and deoxy-Hb show maximum difference while they coincide at 808 nm, the isosbestic point. As such, the PA signal is much more sensitive to changes in blood optical parameters at 680 nm while being insensitive at 808 nm. When they are modulated out of phase, existing system noise or any other background absorption would be significantly suppressed from the system, and the difference between the two signals would be amplified. Therefore, differential PA signals from those two wavelengths allow one to

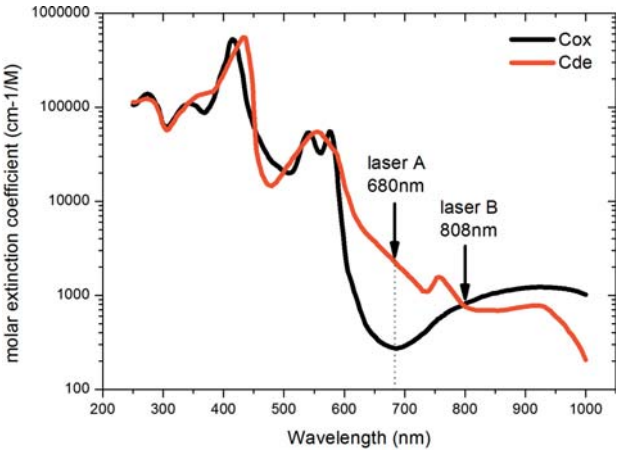

Figure 1 Human Hb molar extinction coefficient spectrum with arrows indicating two wavelengths of interest for the WM-DPAS system; re-plotted from data obtained from [18].

detect very small changes in the carcinogenesis benchmarks with great sensitivity. The theoretical development of WM-DPAS for blood oxygenation and deoxygenation sensing follows.

2.3 Hypoxia monitoring

The Hb absorption coefficient, μ_a, is a function of wavelength and of oxy- and deoxy-Hb concentration (C_{ox} and C_{de}). It can be described as:

$$\mu_a(\lambda, C_{ox}, C_{de}) = \ln(10)\, e_{ox}(\lambda)\, C_{ox} + \ln(10)\, e_{ox}(\lambda)\, C_{de} \quad (7)$$

where e_{ox} and e_{de} are extinction coefficients of oxy- and deoxy-Hb at wavelength λ. Since C_{Hb} is the sum of C_{ox} and C_{de} [19], Eq. (7) can be rearranged as:

$$\mu_a(\lambda, C_{Hb}, C_{ox}) = \ln(10)\, e_{de}(\lambda)\, C_{Hb} + \ln(10) \times [e_{ox}(\lambda) - e_{de}(\lambda)]\, C_{ox} \quad (8)$$

Therefore, for the λ_A = 680 nm laser,

$$\mu_{aA}(C_{Hb}, C_{ox}) = \ln(10)\, e_{de}(\lambda_A) C_{Hb} + \ln(10)\, [e_{ox}(\lambda_A) - e_{de}(\lambda_A)]\, C_{ox} \quad (9)$$

However, for the λ_B = 808 nm laser, the term $[e_{ox}(\lambda_B) - e_{de}(\lambda_B)]$ vanishes since it is at the isosbestic point where $e_{ox}(\lambda_B) = e_{de}(\lambda_B)$ [20]. Therefore, the equation for laser B becomes:

$$\mu_{aB}(C_{Hb}, C_{ox}) = \ln(10)\, e_{de}(\lambda_B)\, C_{Hb} \quad (10)$$

Since $P_A \propto \mu_{aA}$ and $P_B \propto k\mu_{aB}$ (each of the single-ended PA signals is proportional to the absorption coefficient of the sample at the specific wavelengths), Eqs. (9) and (10) can be combined to represent the differential PA signal as:

$$P_{AB} \propto (\mu_{aA} - k\mu_{aB}) = \ln(10)\, [e_{de}(\lambda_A) - k e_{de}(\lambda_B)] \times C_{Hb} + \ln(10)\, [e_{ox}(\lambda_A) - e_{de}(\lambda_A)]\, C_{ox} \quad (11)$$

where P_{AB} is a differential PA signal, μ_{aA} and μ_{aB} are the absorption coefficients of the absorber at specific wavelength A (680 nm) and B (808 nm) respectively, and k is a constant determined by the modulated amplitude ratio $R(A_A/A_B)$ and phase difference $dP(P_A - P_B)$ of the two lasers [20]. In Eq. (11), the constant k can be adjusted as $k e_{de}(\lambda_B) = e_{de}(\lambda_A)$ so that the term $[e_{de}(\lambda_A) - k e_{de}(\lambda_B)]$ becomes 0. In this manner, the differential PA signal is a sole function of C_{ox} [20].

2.4 Pre-malignancy screening

When it comes to pre-malignant tumor detection, it is important to recognize a clear relationship between Hb-dependent biochemical parameters and tissue malignancy. When breast tissues become cancerous, C_{Hb} and StO_2 monotonically increase and decrease, respectively, and those trends can be used for clinical purposes. For cancer diagnostic purposes, therefore, we need the differential PA signal as a function of C_{Hb} and StO_2. The constant k in Eq. (11) needs to be adjusted so that P_{AB} will be dependent primarily on C_{Hb} or StO_2, being free of any non-monotonic effects of C_{ox}. The pre-malignant tumor detection modality does not require making a precise quantification of any of the Hb parameters, but rather the constant k needs to be properly tuned so that the P_{AB} signal fluctuates sensitively only at the suspected pre-malignant tumor site.

3. Materials and methods

3.1 WM-DPAS set-up

The novel WM-DPAS modality utilizes two single frequency modulated (50% duty cycle) optical waveforms with 180.08° and 184.80° phase differences dP, chosen near and far from the out-of-phase condition to study the impact of the phase difference on measurement sensitivity. The two waveforms were 0.3 MHz square-waves modulated at the fixed phase difference by a dual-channel function generator (33522B; Agilent, CA, USA). The modulation frequency was chosen to be away from the transducer peak frequency (1 MHz) to avoid the strong radio frequency (RF) signal interference. Throughout the series of experiments, 0.3 MHz turned out to have the best SNR for this system. The two laser beams that were collimated into 0.8 mm diameters by the same collimators (F230SMA-B; Thorlabs, NJ, USA) were directed to the identical location on the absorber by protected silver mirrors (PF10-03-P01; Thorlabs, NJ, USA). A continuously variable neutral density filter with OD 0.04 – 1 (64-381; Edmund, NJ, USA) was used to sweep the 808-nm laser beam for the differential R-scan. R-scan measurement is achievable by adjusting laser power of either laser. Using the full OD range, the system R ($A_{680\,nm}/A_{808\,nm}$) could be varied from ~0.2 to ~1.8. A single-element 1.0 MHz focused ultrasonic transducer

(V314; Olympus Panametrics, CA, USA) was used as a receiver. The transducer head and the absorber were submerged in de-ionized water for acoustic coupling. The ND filter and the two mirrors were also placed in the water to minimize heat accumulation on the optics. The received differential PA signal was amplified 40 dB by the pre-amplifier (5662; Olympus Panametrics, CA, USA) and analyzed by the hardware lock-in amplifier (SR822; Stanford Research Systems, CA, USA). In this study the 680 nm laser power was fixed at ~1 W. The 808 nm laser power was adjusted between ~0.5 W to ~3.5 W using the continuously variable ND filter (beam diameter: ~15 mm and exposure duration ~15 s for both). The laser power density (0.56 W/cm^2 at 680 nm and 0.28–1.98 W/cm^2 at 808 nm) is currently above the maximum permissible exposure (MPE, 0.2 W/cm^2 at 680 nm and 0.33 W/cm^2 at 808 nm) for this 'proof of concept' study. Once the system is optimized with shorter lasing duration and lower output power, the laser power density will be dropped below the safety level [21].

3.2 *In-vitro blood circulation system set-up*

Sterile heparinized sheep blood (CL2581-500H; ON, CA) was purchased from Cederlane and stored at a 4 °C temperature in the laboratory refrigerator. Before use, each fresh bottle was shaken well to ensure the homogeneity of the blood and then 60 mL of blood were transferred to a 100 mL commercial blood bag with two standard size openings (JB1302; Baxter, IL, USA) using a syringe. This blood bag, originally containing 0.9% sodium chloride solution, was emptied, cleaned with deionized water, and dried thoroughly before storing the blood. After the transfer, the air inside the bag was squeezed out to ensure a complete vacuumed system inside the bag. Once the blood bag was prepared, the remaining part of the *in-vitro* blood circulation system was assembled and a peristaltic pump (Pd5201, Heidolph, Bavaria, DE) introduced suction at one end of the tube operating at 15 rpm. Then, that end of the tube was carefully connected to one opening of the blood bag without introducing air into the system. The sheep blood was allowed to continuously circulate through the system while the pressurized end of the tube was placed in a disposal flask. As all the air in the system was pushed out by the flowing blood, the pressurized end of the tube was carefully connected to the other opening of the blood bag while the pump was still running. The vacuum-sealed blood circulating system was capable of circulating the blood for 7 to 8 hours without causing any blood coagulation. The room temperature was kept at 20 °C at all times. Blood deoxygenation was achieved using sodium dithionite ($Na_2O_4S_2$; Sigma-Aldrich, MO, USA). Based on the published protocol [22], a specific amount of chemical powder was diluted in ~1.5 mL of fresh sheep blood and the diluted solution was slowly injected into the circulation system using a syringe. After allowing 10 minutes for system stabilization, about 0.3 mL of the blood sample were taken out of the system using a new syringe while the pump was temporarily turned off. The blood sample was then uploaded to a B-cassette (OPTImedical, GA, USA) and blood parameters including C_{Hb} and StO_2 of the specific blood sample were confirmed by the commercial blood gas analyzer (CCA-TS; OPTImedical, GA, USA). The used heparinized blood was then diluted with tap water and disposed of down a sanitary drain. The experimental set-up is depicted in Figure 2.

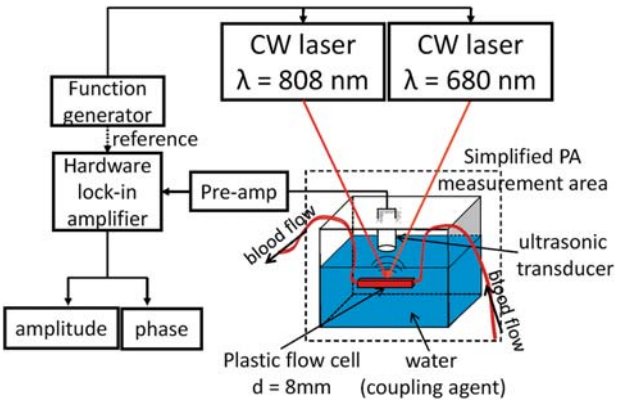

Figure 2 A block diagram of the WM-DPAS system.

4. Results and discussion

For each blood sample with decreasing StO_2, a differential R-scan was performed at different d*Ps* and compared to the corresponding theoretical formalism. The experimental responses showed excellent agreement with the theoretical best-fitting in the range of StO_2 studied for several d*P* settings. Figure 3 shows the *R*-scan results with d*P* = 180.08° (the *R*-scan results with d*P* = 184.80° to investigate the influence of phase difference on measurement sensitivity is provided in the supplement material, see Supporting Information). For more accurate data fitting, the Hb molar extinction coefficient spectrum of adult sheep [23] was adopted. Some parameters used for best-fitting include $v_a = 1.57 \times 10^5$ cm/s, $e_{ox\,A} = 159$ cm^{-1}/M, $e_{de\,A} = 704$ cm^{-1}/M, $e_{ox\,B} = 243$ cm^{-1}/M and $e_{de\,B} = 239$ cm^{-1}/M, where v_a is the speed of sound in the medium, and e_{ox} and e_{de} are the molar extinction coefficients of oxy- and deoxy- sheep blood at the specific wavelengths, respectively.

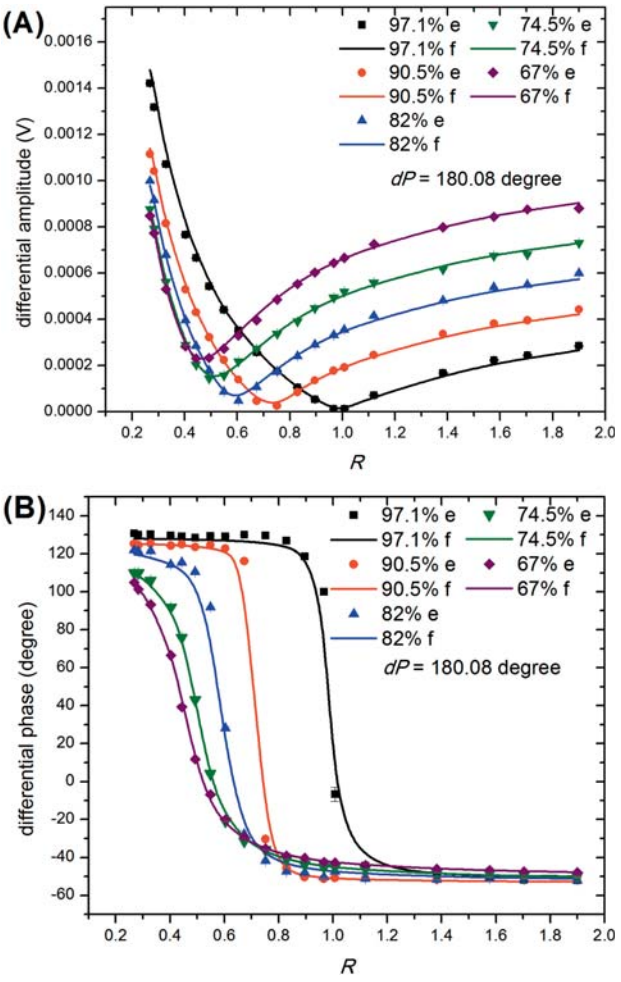

Figure 3 PA differential (**A**) amplitude and (**B**) phase signals over increasing R. System dP was 180.08°. The two lasers were square-wave modulated at 0.3 MHz. e – Experimental, f – Best-fitting.

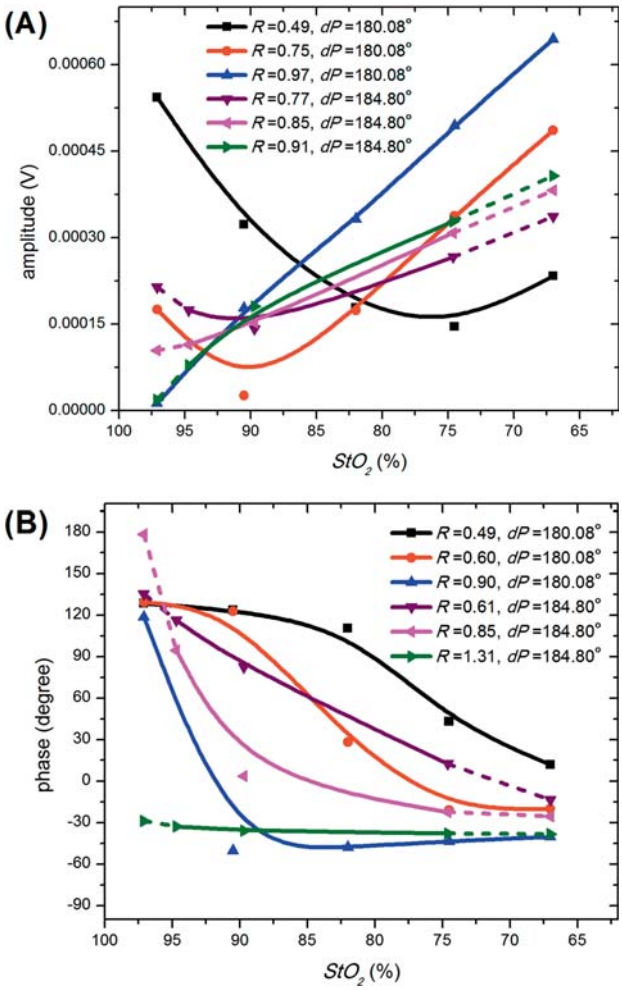

Figure 4 PA differential (**A**) amplitude and (**B**) phase signals with decreasing StO_2 at various R and dP combinations. The two lasers were square-wave modulated at 0.3 MHz. The symbols are experimental data and the lines are guides for the eye.

4.1 WM-DPAS sensitivity tunability

As described in the theoretical section above, sensitivity tuning of the differential PA signal is feasible by adjusting the system R and dP. Figure 4 depicts how differential PA amplitude and phase behavior may vary over decreasing StO_2 according to different combinations of R and dP.

Among numerous possible options, certain R and dP combinations have been identified for practical applications to pre-malignancy detection and hypoxia monitoring.

4.2 Breast pre-malignancy screening

Unlike the PA differential amplitude signal which gradually changes over the StO_2 range, the PA differential phase signal can be tuned to shift around a certain StO_2 value for screening. For pre-malignancy detection purposes, the WM-DPAS system needs to be tuned at R and dP in a range where the signal from the pre-malignant sample fluctuates sensitively. Out of the eight samples tested (StO_2 = 97.5%, 91.5%, 89.6%, 85.7%, 81%, 76%, 68.6% and 39.8%), the blood sample with 85.7% StO_2 was assumed to be pre-malignant. It should be emphasized that the sample with 85.7% StO_2 was arbitrarily chosen to be pre-malignant in this study, but the WM-DPAS *sensitivity tunability* suggests that the system R and dP can be freely tuned so that maximum-sen-

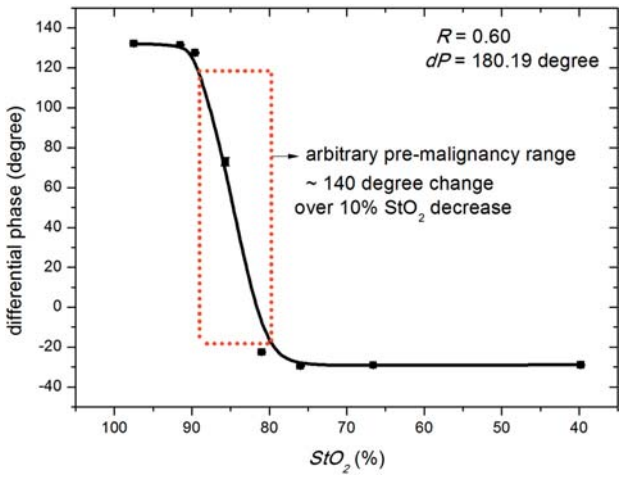

Figure 5 PA differential phase signal change as StO_2 decreased from 97.5% to 39.8% when R = 0.60 and dP = 180.19°. The system showed drastic phase shift over 10% StO_2 decrease as indicated by the dashed square.

sitivity differential phase transition occurs in the specific range of interest (because different organs have different pre-malignant thresholds) [24, 25]. The system was tuned correspondingly at R = 0.60 and dP = 180.19°.

As shown in Figure 5, a clearer step-function-like shape was obtained which exhibited about 140° phase shift over only a 10% StO_2 decrease while small or no phase shifts were observed at higher (healthy) and lower (malignant) ends of the graph. This suggests that the differential phase of the WM-DPAS system can be used to sensitively detect pre-malignant tumors based on their optical properties.

4.3 Hypoxia monitoring

The tunability of the WM-DPAS system also suggests that both the differential amplitude and phase signals could be used for the quantitative measurement of breast carcinogenesis benchmarks, especially StO_2. For each channel, optimal R and dP were chosen in a range showing strong correlation with StO_2 and high sensitivity.

For the differential amplitude, R = 0.97 and dP = 180.08° was optimal as it exhibited strong correlation with StO_2 and about 162.84% signal change per 1% StO_2. As depicted in Figure 6A, such sensitivity was significant when it was compared to the single-ended response in which the 680 nm and 808 nm measurements showed only 4.76% and 0.54% signal change per 1% StO_2, respectively. Similarly for the differential phase, R = 0.61 and dP = 184.80° were chosen for 1% StO_2 showing strong correlation with StO_2 and high sensitivity of 5.19° change per 1% StO_2. As

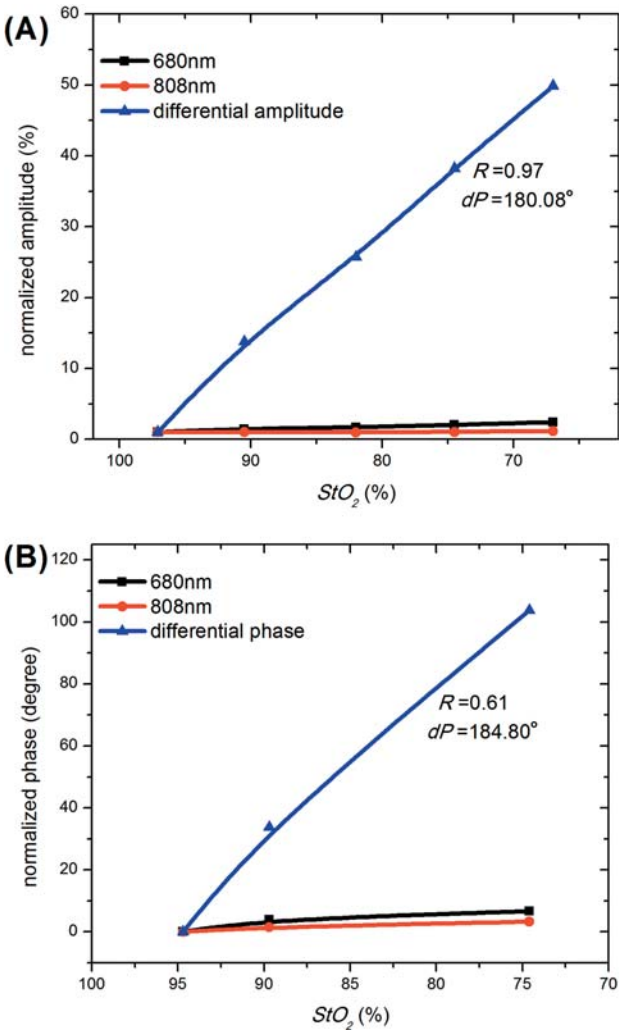

Figure 6 Sensitivity comparison of (**A**) optimally tuned differential amplitude and (**B**) phase signals with corresponding single-ended signals.

shown in Figure 6B, the single-ended 680 nm and 808 nm measurements only showed 0.33° and 0.17° change per %StO_2.

The superior sensitivity of the WM-DPAS system is outstanding when it is compared to other non-invasive techniques that have been used for quantitative StO_2 measurements as shown in Table 1. Additionally, instead of relying on single amplitude channels like the existing modalities, the WM-DPAS use of two complementary amplitude and phase channels further enhances the reliability of hypoxia monitoring. In this study, only a few combinations of R and dP were explored. Therefore, it is expected that the hypoxia monitoring capability of the WM-DPAS system could be further optimized in future with finer tuning of R and dP.

Table 1 Signal sensitivity comparison of various non-invasive StO_2 quantification modalities.

Ref.	method	channel	unit signal change	target
This study	WM-DPAS; CW laser with 680 nm and 808 nm diodes	amplitude phase	162.84%/% StO_2 5.19°/% StO_2	*in-vitro* sheep blood
[26]	PACT; pulsed laser with 680 nm modulation	amplitude	2.51%/% StO_2	*in-vivo* mouse
[14]	PAS; pulsed laser with 760 nm modulation	amplitude	1.06%/% StO_2	*in-vivo* human blood
[27]	PAM; pulsed laser with 570 nm modulation	amplitude	0.12%/% StO_2	*in-vivo* Phantom (cornstarch + gelatin)

Supporting Information

Additional supporting information may be found in the online version of this article at the publisher's website.

Acknowledgements A.M. gratefully acknowledges the support of the Alexander von Humboldt Foundation for a Re-invited Visiting Professor Award during his sabbatical leave at the Helmholtz Zentrum München, Institut für Biologische und Medizinische Bildgebung. He also acknowledges a CIHR-NSERC Collaborative Health Research Project (CHRP) award, the Canada Research Chairs (CRC) program. A. M. and S(S). C. acknowledge a Samsung Advanced Institute of Technology Global Research Outreach ("GRO") award.

Author biographies Please see Supporting Information online.

References

[1] J. Walsh, A. Lebedev, E. Aten, K. Madsen, L. Marciano, and H. Kolb, Antioxid Redox Signaling **21**, 1516–1531 (2014).
[2] M. Hockel and P. Vaupel, J. Natl. Cancer Inst. **93**, 266–276 (2001).
[3] A. Cyrous, B. O'Neal, and W. D. Freeman, Expert Rev. Neurother. **12**, 915–928 (2012).
[4] P. Vaupel, M. Hockel, and A. Mayer, Antioxid. Redox. Signal **9**, 1221–1235 (2007).
[5] J. Dengler, C. Frenzel, P. Vajkoczy, S. Wolf, and P. Horn, Intensive Care Med. **37**, 1809–1815 (2011).
[6] H. Yasui, S. Matsumoto, N. Devasahayam, J. P. Munasinghe, R. Choudhuri, K. Saito, S. Subramanian, J. B. Mitchell, and M. C. Krishna, Cancer Res. **70**, 6427–6436 (2010).
[7] C. P. Lee, G. S. Payne, A. Oregioni, R. Ruddle, S. Tan, F. I. Raynaud, D. Eaton, M. J. Campbell, K. Cross, and G. Halbert, M. Tracy, J. McNamara, B. Seddon, M. O. Leach, P. Workman, and I. Judson, Br. J. Cancer **101**, 1860–1868 (2009).
[8] S. Matsumoto, H. Yasui, S. Batra, Y. Kinoshita, M. Bernardo, J. P. Munasinghe, H. Utsumi, R. Choudhuri, N. Devasahayam, S. Subramanian, J. B. Mitchell, and M. C. Krishna, Proc. Natl. Acad. Sci. USA **106**, 17898–17903 (2009).
[9] G. Casey, Nurs. Stand. **15**, 46–53 (2001).
[10] S. D. Konecky, R. Choe, A. Corlu, K. Lee, R. Wiener, S. M. Srinivas, J. R. Saffer, R. Freifelder, J. S. Karp, N. Hajjioui, F. Azar, and A. G. Yodh, Med. Phys. **35**, 446–455 (2008).
[11] M. Li, J. Oh, X. Xie, G. Ku, W. Wang, C. Li, G. Lungu, G. Stoica, and L. V. Wang, Proc. IEEE **96**, 481–489 (2008).
[12] K. Stanz, B. Liu, C. Minsong, D. Reinecke, K. Miller, and R. Kruger, SPIE Proc. **6086**, 605–608 (2006).
[13] B. Cox, J. G. Laufer, S. R. Arridge, and P. C. Beard, J. Biomed. Opt. **17**, 061202 (2012).
[14] J. Laufer, D. Delpy, C. Elwell, and P. Beard, Phys. Med. Biol. **52**, 141–168 (2007).
[15] A. Q. Bauer, R. E. Nothdurft, T. N. Erpelding, L. V. Wang, and P. Culver, J. Biomed. Opt. **16**, 096016 (2011).
[16] Z. Guo, S. Hu, and L. V. Wang, Opt. Lett. **35**, 2067–2069 (2010).
[17] S. Telenkov, R. Alwi, and A. Mandelis, Rev. Sci. Instrum. **84**, 104907 (2013).
[18] R. Splinter and B. A. Hooper, An Introduction to Biomedical Optics (CRC press, Boca Raton, 2006).
[19] N. Shah, A. E. Cerussi, D. Jakubowski, D. Hsiang, J. Butler, and B. J. Tromberg, J. Biomed. Opt. **9**, 534–540 (2004).
[20] S. Choi, A. Mandelis, X. Guo, B. Lashkari, S. Kellnberger, and V. Ntziachristos, Int. J. Thermophys. DOI: 10.1007/s10765-014-1710-5 (2014)
[21] American National Standards Institute (ANSI) ANSI Z136.1–1993: 42–44 (1993).
[22] K. Briley-Sæbø and A. Bjørnerud, Proc. Intl. Soc. Mag. Reson. Med. **8**, 2025 (2000).
[23] W. G. Zijlstra, A. Buursma, and O. W. van Assendelft, Visible and Near Infrared Absorption Spectra of Human and Animal Haemoglobin: Determination and Application (VSP BV, Boston, 2000).
[24] R. L. P. van Veen, A. Amelink, M. Menke-Pluymers, C. van der Pol, and H. J. C. M. Sterenborg, Phys. Med. Biol. **50**, 2573–2581 (2005).
[25] H. Wang, J. Jiang, C. Lin, G. Huang, and J. Yu, Opt. Express **17**, 2805–2817 (2009).
[26] J. Xia, A. Danielli, Y. Liu, L. Wang, K. Maslov, and L. V. Wang, Opt. Lett. **38**, 2800–2803 (2013).
[27] Y. Jiang, A. Forbrich, T. Harrison, and R. J. Zemp, J. Biomed. Opt. **17**, 036012 (2012).
[28] K. Kwon, and S. Park, Sensor. Actuator. **43**, 49–54 (1994).